The American Journal of Pathology, Vol. 190, No. 8, August 2020

The American Journal of PATHOLOGY
ajp.amjpathol.org

See related Commentary on page 1622

TUMORIGENESIS AND NEOPLASTIC PROGRESSION

Discoidin Domain Receptor 1 (DDR1) Is Necessary for Tissue Homeostasis in Pancreatic Injury and Pathogenesis of Pancreatic Ductal Adenocarcinoma

Jeanine M. Ruggeri,[*†‡] Janusz Franco-Barraza,[§] Anjum Sohail,[¶‖] Yaqing Zhang,[**‡] Daniel Long,[*‡] Marina Pasca di Magliano,[**‡] Edna Cukierman,[§] Rafael Fridman,[¶‖††] and Howard C. Crawford[*†**]

From the Departments of Molecular and Integrative Physiology, Internal Medicine,† and Surgery** and the Rogel Comprehensive Cancer Center,‡ University of Michigan, Ann Arbor, Michigan; Departments of Pathology¶ and Oncology†† and the Karmanos Cancer Institute,‖ Wayne State University, Detroit, Michigan; and the Marvin and Concetta Greenberg Pancreatic Cancer Institute,§ Fox Chase Cancer Center, Philadelphia, Pennsylvania*

Accepted for publication March 26, 2020.

Address correspondence to Rafael Fridman, Ph.D., Departments of Pathology and Oncology, Wayne State University, 540 E. Canfield Ave, Detroit, MI 48201; or Howard C. Crawford, Ph.D., Departments of Molecular and Integrative Physiology, Internal Medicine, and Surgery, University of Michigan, 1500 E. Medical Center Dr., Ann Arbor, MI 48109. E-mail: rfridman@med.wayne.edu or howcraw@med.umich.edu.

Pancreatic ductal adenocarcinoma (PDA) and chronic pancreatitis are characterized by a dense collagen-rich desmoplastic reaction. Discoidin domain receptor 1 (DDR1) is a receptor tyrosine kinase activated by collagens that can regulate cell proliferation, migration, adhesion, and remodeling of the extracellular matrix. To address the role of DDR1 in PDA, Ddr1-null ($Ddr^{-/-}$) mice were crossed with the $Kras^{G12D/+}$; $Trp53^{R172H/+}$; $Ptf1a^{Cre/+}$ (*KPC*) model of metastatic PDA. $Ddr1^{-/-}$; *KPC* mice progress to differentiated PDA but resist progression to poorly differentiated cancer compared with *KPC* control mice. Strikingly, severe pancreatic atrophy accompanied tumor progression in $Ddr1^{-/-}$; *KPC* mice. To further explore the effects of Ddr1 ablation, $Ddr1^{-/-}$ mice were crossed with the $Kras^{G12D/+}$; $Ptf1a^{Cre/+}$ neoplasia model and subjected to cerulein-induced experimental pancreatitis. Similar to *KPC* mice, tissue atrophy was a hallmark of both neoplasia and pancreatitis models in the absence of Ddr1. Compared with controls, $Ddr1^{-/-}$ models had increased acinar cell dropout and reduced proliferation with no difference in apoptotic cell death between control and $Ddr1^{-/-}$ animals. In most models, organ atrophy was accompanied by increased fibrillar collagen deposition, suggesting a compensatory response in the absence of this collagen receptor. Overall, these data suggest that DDR1 regulates tissue homeostasis in the neoplastic and injured pancreas. *(Am J Pathol 2020, 190: 1735–1751; https://doi.org/10.1016/j.ajpath.2020.03.020)*

Pancreatic ductal adenocarcinoma (PDA) is currently the third leading cause of cancer deaths in the United States, affecting >57,000 adults each year.[1] Only 10% of patients with PDA survive up to 5 years, with most patients succumbing to the disease within a year of diagnosis.[1,2] The high mortality of PDA is attributed to the absence of distinct clinical symptoms, a lack of early detection methods, and ineffective therapeutic options.[3] During the past few decades, considerable advancements have been made in studying the development of PDA, but the prognostic outcome has improved only marginally. Consequently, further understanding of the molecular events that contribute to the initiation and progression of PDA is essential for the prevention and early discovery of this lethal disease.

Chronic pancreatitis (CP) increases the lifetime risk of developing PDA.[4] CP is characterized by permanent damage to the pancreas with progressive loss of exocrine cell

Supported by NIH grants U01CA2241145 (H.C.C. and M.P.d.M.), R50CA232985 (Y.Z.), and R21CA191347 (H.C.C and R.F.); Department of Defense grants CA170568 (H.C.C. and R.F.) and R21CA231252 and R01CA232256 (E.C.); Core Grants P30CA046592 (Rogel Cancer Center) and P30CA06927 (Fox Chase Cancer Center); a Sky Foundation development grant (H.C.C. and R.F.); Pennsylvania's Department of Health Research Formula Funds (E.C.); and the Fifth District AHEPA Cancer Research Foundation (E.C.).

Disclosures: None declared.

https://doi.org/10.1016/j.ajpath.2020.03.020

function, inflammation, and a prominent fibrotic response accompanied by acinar-ductal metaplasia (ADM).[4,5] ADM is a transdifferentiation event in which acinar cells acquire a ductal cell–like phenotype that plays a reparative role in pancreatic injury.[5,6] With the acquisition of activating *KRAS* mutations, ADM can progress to premalignant pancreatic intraepithelial neoplasia (PanIN).[7,8] As additional mutations accumulate, PanINs are hypothesized to advance to invasive PDA.[9,10]

Both CP- and *KRAS*-driven tumorigeneses share similar morphologic features, such as the prominent collagen-dense desmoplastic response that displaces the normal epithelium.[9–11] The overproduction of collagen, in concert with the deposition of other extracellular matrix (ECM) proteins, creates a largely impenetrable, hypoxic, and nutrient-deficient environment that is influenced by ECM remodeling and impedes drug delivery.[12] The overwhelming desmoplastic response has propelled studies that target components of the stroma, such as hyaluronan, to enhance drug delivery.[13] Other studies have targeted the desmoplastic fibroblasts, which are a major source of collagen production.[14–17] Unfortunately, widespread depletion of fibroblasts or deletion of specific signaling networks in fibroblast activation accelerates PDA progression.[15,16] However, reprogramming fibroblasts to a quiescent state after tumors have improved drug delivery in preclinical models of PDA.[17] Although the extensive collagen deposition is a hallmark of pancreatic disease, its role during the onset and progression of CP and PDA remain inconclusive. The discrepancies in the current literature not only provide evidence for the complex role the stroma plays in pancreatic disease but also showcase the diverse interactions of stromal factors that can have opposing roles in PDA progression.

Discoidin domain receptor 1 (DDR1) is a type 1 transmembrane receptor tyrosine kinase that uses collagens as cognate ligands to regulate cell proliferation, adhesion, and migration, and plays a role in ECM remodeling.[18] Aberrant activation of DDR1 contributes to a number of pathologic conditions, such as lung and kidney fibrosis.[19,20] DDR1 is also up-regulated in various cancers, including PDA, and plays a role in tumor growth, progression, and metastasis.[21–23] Pharmacologic inhibition of DDR1 prolongs survival in a PDA mouse model, but its role in pancreatitis and early neoplasia has not been explored.[23] In this study, we used Ddr1-null ($Ddr1^{-/-}$) mice to elucidate its functions during the onset and progression of pancreatic cancer as well as pancreatitis. These data demonstrate a novel role for DDR1 as a gatekeeper of tissue homeostasis because its ablation in each of these models leads to severe tissue atrophy marked by reduced proliferation and altered ECM dynamics.

Materials and Methods

Mouse Models

The following mice were used: $Ddr1^{-/-}$ mice (as previously characterized[24]); $Kras^{LSL\text{-}G12D/+}$; $Ptf1a^{Cre/+}$ (KC); $R26R^{LSL\text{-}YFP}$ for tumorigenesis studies; and $Kras^{LSL\text{-}G12D/+}$; $Trp53^{R172H/+}$ $Ptf1a^{Cre/+}$; $R26R^{LSL\text{-}YFP}$ for metastasis.[16,25,26] All animal protocols were reviewed and approved by the University of Michigan Institutional Animal Care and Use Committee.

Cell Culture

Human pancreatic cancer cell lines (AsPC-1, PANC-1, MiaPaCa-2, Capan-1, CFPAC-1, and BxPC-3) were purchased from the ATCC (Manassas, VA). Cells were cultured in Dulbecco's modified Eagle's medium (Thermo Fisher Scientific, Waltham, MA) or RPMI 1640 medium (Thermo Fisher) containing 10% fetal bovine serum and maintained at 37°C in a humidified incubator with 5% CO_2 and 95% air.

Cerulein Treatment

Experimental pancreatitis was induced, as previously described,[27] by administering 250 μg/kg of cerulein (46-1-50; American Peptide Company Inc., Sunnyvale, CA) intraperitoneally twice daily for 2 weeks and allowed to recover for 1, 3, 7, and 14 days in control and $Ddr1^{-/-}$ littermates. Mice used in this study were 8 to 12 weeks old with weights between 18 and 25 g. Saline (catalog number 07982-100TAB-F; Sigma-Aldrich, St. Louis, MO) was used as a negative control for cerulein. For pancreatitis-induced tumorigenesis, 6-week–old *KC* and $Ddr1^{-/-}$; *KC* littermates were treated with 250 μg/kg of cerulein once daily for 5 consecutive days and allowed to recover for 1, 4, and 6 weeks before tissue harvesting.

IHC, Immunofluorescence, and Quantification

Distribution and use of all human samples were approved by the institutional review boards of the Mayo Clinic. For immunohistochemistry (IHC), pancreata were removed and fixed in Z-fix (catalog number NC9050753; Anatech Ltd., Battle Creek, MI) overnight. Tissues were processed using a Leica ASP300S tissue processor (Leica Microsystems Inc., Buffalo Grove, IL). Paraffin-embedded tissues were sectioned at 4 μm and stained for specific target proteins using the Discovery Ultra XT autostainer (Ventana Medical Systems Inc., Tucson, AZ), with antibodies as listed in Table 1, and counterstained with Mayer's hematoxylin (catalog number NC9220898; Sigma-Aldrich). Hematoxylin and eosin (H&E) staining was performed using Mayer's hematoxylin solution and Eosin Y (catalog number HT110116; Thermo Fisher Scientific, Pittsburgh, PA). Picrosirius Red staining was performed according to the manufacturer's instructions (Polysciences Inc., Warrington, PA). Gomori's Trichrome stain was performed according to the manufacturer's instructions (Thermo Fisher Scientific and Richard-Allan Scientific, San Diego, CA). IHC slides were then scanned on a Pannoramic SCAN scanner (Perkin

Table 1 Antibodies Used in This Study

Antibody	Company	Catalog no.	Concentration	Method
DDR1 (C-20)	Santa Cruz Biotechnology, Dallas, TX	sc532	1:250	Human tissue microarray
DDR1 (D16G) XP	Cell Signaling Technologies, Danvers, MA	5583	1:250	Immunofluorescence
			1:1000	Western blot
Ki-67	Abcam, Cambridge, United Kingdom	ab15580	1:1000	Immunohistochemistry
Cleaved caspase 3	Cell Signaling Technologies	9664	1:200	Immunohistochemistry
Phosphohistone H3 (Ser10)	Cell Signaling Technologies	9701	1:100	Immunohistochemistry and immunofluorescence
Amylase	Sigma, St. Louis, MO	A8273	1:1000	Immunohistochemistry
Amylase	Santa Cruz	sc12821	1:250	Immunofluorescence
Cytokeratin 19	TROMA, Long Island, NY	Max Plank	1:1000	Immunohistochemistry
E-cadherin	BD Pharmingen, Franklin Lakes, NJ	610182	1:100	Immunofluorescence
P21	Santa Cruz	sc471	1:100	Immunohistochemistry
DDR2	Cell Signaling Technologies	12133	1:1000	Western blot
Collagen 1a	Abcam	Ab34710	1:250	Immunohistochemistry
Collagen 1a	Millipore, Burlington, MA	Ab765p	1:1000	Western blot
α-Smooth muscle actin	Abcam	Ab5694	1:20,000	Western Blot
Podoplanin (biotinylated)	BioLegend, San Diego, CA	127403	1:100	Immunofluorescence

DDR1, discoidin domain receptor 1; DDR2, discoidin domain receptor 2.

Elmer, Seattle, WA). Scanned images were quantified using algorithms provided from Halo software version 2.0 (Indica Labs, Corrales, NM).

Immunofluorescence was performed on pancreata that were fixed in Z-fix for 2 hours, followed by an overnight float in 30% sucrose. Pancreata were incubated in a 1:1 mixture of 30% sucrose and OCT embedding medium for 1 hour, embedded in OCT, frozen in liquid nitrogen, and stored at −80°C. Tissue sections (7 μm) were permeabilized in 1× phosphate-buffered saline (PBS) supplemented with 0.1% Triton X-100 (catalog number T9284; Sigma-Aldrich) for 1 hour and blocked in 1× PBS supplemented with 5% donkey serum and 1% bovine serum albumin for 1 hour. Sections then were incubated with primary antibody diluted in 1× PBS supplemented with 0.1% Triton X-100 and 1% bovine serum albumin overnight at room temperature, followed by 3 washes in 0.1% Triton X-100/PBS for a total of 1 hour. Sections were incubated with secondary antibodies conjugated with Alexa Fluor (Invitrogen, Carlsbad, CA) for 1 hour at room temperature, followed by 3 washes in 0.1% Triton X-100/PBS. Hoechst 33342 stain (catalog number 62249 Thermo Fisher Scientific) was used for nuclear stain at 1:10,000 dilution in 1× PBS solution for 20 minutes. Slides were rinsed in deionized water and mounted with Prolong Diamond antifade mount (catalog number P36961; Thermo Fisher Scientific). Images presented were acquired on a confocal microscope LSM800 (Zeiss, Oberkochen, Germany). Immunofluorescence slides were scanned and quantified as with IHC-stained slides.

Immunoblotting

Mouse pancreas whole tissue lysates for protein analysis were obtained by removing a small piece of the pancreas from mice after euthanasia and snap freezing in liquid nitrogen. Tissue samples were then homogenized using the Pro 250 Homogenizer (Pro Scientific Inc., Oxford, CT) in radioimmunoprecipitation assay buffer supplemented with protease inhibitor cocktail (catalog number PIA32965; Thermo Fisher Scientific) and PhosSTOP phosphatase inhibitor cocktail (catalog number 4906845001; Sigma-Aldrich). Lysates were cleared by centrifugation and stored at −80°C. Human cell lines were lysed with radioimmunoprecipitation assay buffer and cleared by centrifugation. Protein concentrations were determined using the BCA Protein Assay Kit (catalog number PI23228; Thermo Fisher Scientific). Proteins were separated using SDS-PAGE and transferred to a polyvinylidene difluoride membrane (catalog number IPVH00010; VWR, Radnor, PA). Primary antibodies used are listed in Table 1. Secondary antibody coupled to horseradish peroxidase (GE Healthcare, Pittsburgh, PA) and the enhanced chemiluminescence detection system (BioRad Clarity and Max Western ECL Substrate, BioRad Laboratories, Hercules, CA) were used to visualize proteins using the BioRad ChemiDoc Imaging System (BioRad Laboratories).

Second Harmonic Generation (SHG) of Polarized Light Microscopy

Imaging acquisition of polymerized/fibrillar collagen was attain using the Leica SP8 DIVE confocal/multiphoton microscope system (Leica Microsystems Inc.) mounted with a 25X HC FLUOTAR L 25x/0.95NA W VISIR water-immersion objective and illuminating, at 850 nm, with IR laser Chameleon Vision II (Coherent Inc., Santa Clara, CA). Backward emission settings were used to generate signals collected via a nondescanned detector configured to register 410- to 440-nm wavelengths. Three areas were selected per H&E-stained slide (*Materials and Methods*). Each selected

area was acquired by collecting three images or regions (eg, $n = 9$ per H&E slide). Acquired regions used identical settings and were recorded as monochromatic, 16-bit image stacks set to 4-μm Z distances, using the Leica Application Suite X version 3.5.5 software (Leica Microsystems Inc.). Digital imaging analyses were conducted with FIJI software (Image version 1.52p; Eliceiri/LOCI Group, University of Madison, Madison, WI). Raw image stacks were three-dimensional reconstituted as maximum projections. Signal to noise thresholds were set identically for all images. Positive (eg, threshold) signal areas were used to calculate integrated second harmonic generation (SHG) intensities (eg, SHG signal/SHG area). Wild-type (*WT*) mean integrated intensity values were used for normalization; results represent arbitrary units compared with *WT* controls. Selected, representative images shown in figures correspond to SHG signal intensity maps in which the reconstituted monochromatic images are shown as pseudo-colored representations in which cold colors indicate high SHG signal.

Pathologic Analysis

Human tissue microarrays and murine PDA samples were graded blindly (Y.Z).

Statistical Analysis

Individual data points were plotted using Prism software version 8.0.2 (GraphPad Software Inc., San Diego, CA) for which the mean (SD) were calculated. Significance was determined using a two-tailed *t*-test for the comparison between two groups. $P < 0.05$ was considered statistically significant.

Results

DDR1 Is Expressed in Tumor Epithelia in Human PDA and Murine Models of PDA

To evaluate the expression of DDR1 in PDA, IHC was performed on human pancreatic cancer tissue microarrays. Consistent with previous studies, robust DDR1 expression was found at the plasma membrane of neoplastic lesions (Figure 1A) and low to no expression of DDR1 in poorl -differentiated tumors (Figure 1A).[23] DDR1 was also expressed in several established human PDA cell lines, with the lowest expression being found in the poorly differentiated MIA PaCa-2 and PANC-1 lines (Figure 1B).[23]

To explore the expression of DDR1 in a metastatic PDA mouse model, the $Kras^{LSL\text{-}G12D/+}$; $Trp53^{LSL\text{-}R172H/+}$; $Ptf1a\text{-}^{Cre/+}$; $Rosa26R^{LSL\text{-}YFP/+}$ (*KPCY*) mouse model was used.[16,26] The *KPCY* model recapitulates many of the key features of the human disease, including progression through precancerous neoplasia together with a co-evolving collagen-dense fibrotic stroma and metastasis primarily to the liver and lungs.[16,26] The $ROSA26R^{LSL\text{-}YFP}$ allele allows for lineage tracing of the epithelial cells throughout tumor progression.[16] In the *KPCY* pancreas, Ddr1 was expressed at the membrane of well- to moderately differentiated PDA, similar to what we observed in human samples (Figure 1C).

DDR1 Promotes Tumor Growth and Progression

To define the role of DDR1 in PDA progression, $Ddr1^{-/-}$ mice were crossed with the *KPC* model (Supplemental Figure S1A).[24,26,28] $Ddr1^{-/-}$ animals have been previously characterized and have no defects in pancreas development.[24,28] To study the effects of DDR1 ablation in PDA, *KPC* and $Ddr1^{-/-}$; *KPC* mice were aged until moribund and then sacrificed. Within these parameters, control animals succumbed to complications of PDA between 24 and 39 weeks. Two $Ddr1^{-/-}$; *KPC* mice were sacrificed because of hind limb paralysis at 26 weeks of age, an independent morbidity occasionally evident with the $Ptf1a^{Cre/+}$ driven *KPC* model due to brain and spinal tumor development (J.M.R., J.F.-B., A.S., Y.Z., D.L., M.P.d.M., E.C., R.F., and H.C.C., unpublished data). The remaining $Ddr1^{-/-}$; *KPC* mice became moribund between 21 and 40 weeks of age, with one mouse that remained symptom free up to 42 weeks, at which point the experiment was terminated (Supplemental Figure S1B).

Although no differences were observed in overall survival between the two cohorts, gross examination and quantitation of pancreatic mass (PM) revealed that $Ddr1^{-/-}$; *KPC* mice had significantly smaller pancreata compared with *KPC* controls of the same age (Figure 2, A and B; Supplemental Figure S1C). Western blot analysis of pancreatic tissue lysates confirmed Ddr1 expression in *KPC* cohorts and its absence in $Ddr1^{-/-}$; *KPC* tissue (Supplemental Figure S1D). Necropsy revealed that 4 of 6 KPC mice had visible liver metastases compared with only 1 of 7 $Ddr1^{-/-}$; *KPC* mice (1 of 5 that made it to the end point without paralysis) (Figure 2C). Histologic examination showed that all *KPC* tumors had progressed to moderately or poorly differentiated adenocarcinoma (Figure 2D and Table 2). $Ddr1^{-/-}$; *KPC* mice, in contrast, presented with well- to moderately differentiated adenocarcinoma, with the exception of the one animal with liver metastases, which also presented with a poorly differentiated primary tumor (Figure 2D, Table 2). Although paralysis limited our cohort size, the findings that $Ddr1^{-/-}$; *KPC* mice generally do not present with metastatic disease are consistent with pharmacologic inhibition of DDR1 inhibiting PDA progression in a similar model.[23]

On the basis of the consistent phenotype of a smaller pancreas found in the $Ddr1^{-/-}$; *KPC* cohort regardless of histologic grade, we hypothesized that $Ddr1^{-/-}$ tissue had a defect in cell proliferation or survival. Because *KPC* mice commonly progressed to poorly differentiated tumors, which were always more proliferative than the well- and moderately differentiated tumors from either cohort (Figure 2D), only differentiated tumors from both genotypes

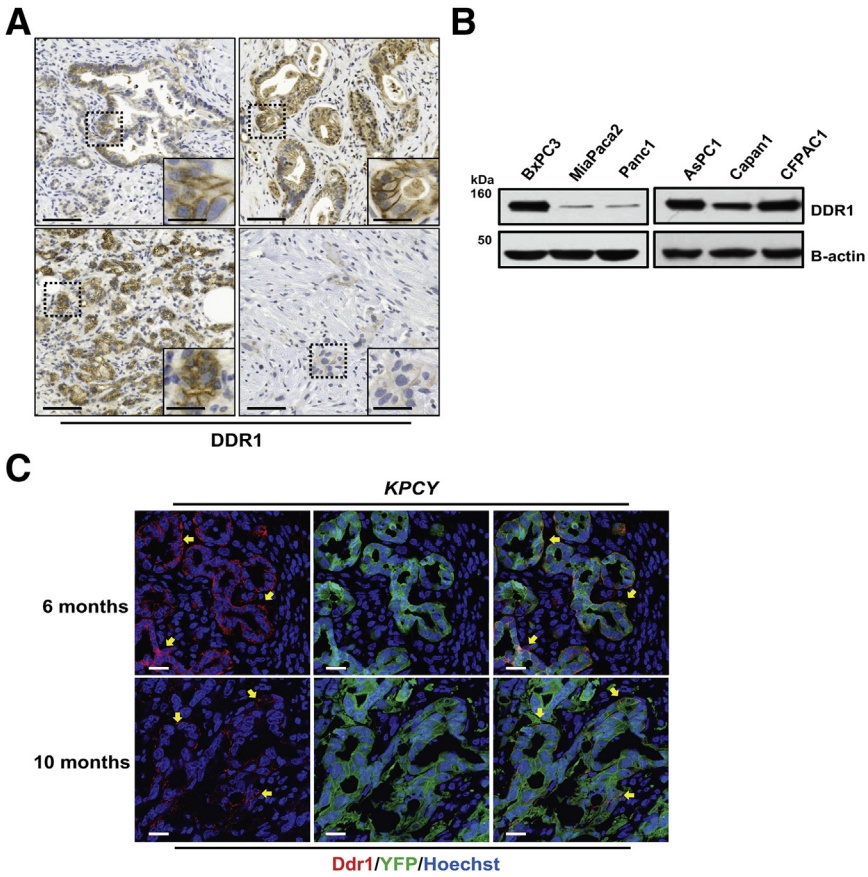

Figure 1 Discoidin domain receptor 1 (DDR1) is upregulated in human pancreatic ductal adenocarcinoma (PDA) and murine models of PDA. **A:** Immunohistochemistry for DDR1 on representative human PDA samples. **B:** Western blot of DDR1 expression in human PDA cell lines. **C:** Indirect immunofluorescence detection of Ddr1 (red) observed localized at the membrane of neoplasia in the *Kras*$^{LSL\text{-}G12D/+}$; *Trp53*$^{LSL\text{-}R172H/+}$; *Ptf1a*$^{Cre/+}$; *Rosa26R*$^{LSL\text{-}YFP/+}$ (*KPCY*) mouse model of PDA at 6 and 10 months. Yellow fluorescent protein (YFP) lineage tracer (green) and Hoechst (blue) for nuclear staining are shown. **Boxed areas** are shown at higher magnification in the **insets**. **Yellow arrows** indicate Ddr1^{+} lesions. Scale bars: 100 μm (**A**); 25 μm (**A**, **insets**); 20 μm (**C**).

were directly compared for quantitative analyses (Figure 2E). *Ddr1*$^{-/-}$*; KPC* tumors had significantly fewer Ki-67^{+} proliferative cells than *KPC* tumors (Figure 2, D and E). Phosphohistone H3 (p-hH3) staining was used as an independent measure of cell proliferation and confirmed that *Ddr1*$^{-/-}$*; KPC* tumors were less proliferative than *KPC* controls (Figure 2, D and E). *Ddr1*$^{-/-}$*; KPC* tumors also had drastically fewer cleaved caspase 3 (CC3)$^{+}$ cells, suggesting that tissue atrophy was not attributable to greater apoptotic cell death in these pancreata (Figure 2, D and E).

In addition to the morphologic changes within the epithelium, PDA is defined by a collagen-dense fibrotic response associated with tumor progression and malignancy.[29] To determine whether the loss of DDR1 affects fibrosis, tissues were stained with Gomori's Trichrome (blue) and Picrosirius Red stains. The relative amounts of both stains were significantly elevated in *Ddr1*$^{-/-}$*; KPC* mice compared with controls (Figure 3A, Supplemental Figure S1E), suggesting more overall collagen and tissue fibrosis. SHG of polarized light microscopy was then used to visualize polymerized (eg, mature) collagen fibers. The overall SHG integrated intensity was higher in *Ddr1*$^{-/-}$*; KPC* mice consistent with the histologic collagen-indicative stains (Figure 3B).

Collectively, these data suggest that the presence of DDR1 interacts with collagens to promote tumor progression, potentially associated with a tumor-restraining type of tissue fibrosis. The associated subsequent smaller, less proliferative pancreas observed in the *Ddr1*$^{-/-}$*; KPC* mice may lead to pancreatic insufficiency, contributing to their decline even with only low metastatic disease.

DDR1 Ablation Induces Tissue Atrophy in Early Pancreatic Neoplasia

A possible explanation for the observed pancreatic atrophy in the *Ddr1*$^{-/-}$*; KPC* mice is that normal pancreatic tissue is dying at an earlier point in tumor progression, a possibility that could be missed by analyzing tissues only at the end point. To test this hypothesis, the effect of DDR1 ablation was investigated during early tumor development. For this purpose, the *KC* model of pancreatic neoplasia was used, which is known to recapitulate the early stages of carcinogenesis in a predictable manner.[25] In this model, endogenous expression of DDR1 is relatively low within healthy acinar regions (Supplemental Figure S2A). However, DDR1 was found to be highly expressed in the epithelia of ADM and PanINs (Figure 4A, Supplemental Figure S2A).[25]

To study the role of DDR1 during the onset of pancreatic tumorigenesis, *Ddr1*$^{-/-}$ mice were crossed with the *KC* model to generate *Ddr1*$^{-/-}$*; KC* mice (Supplemental Figure S2B). PM relative to total body weight (BW) was

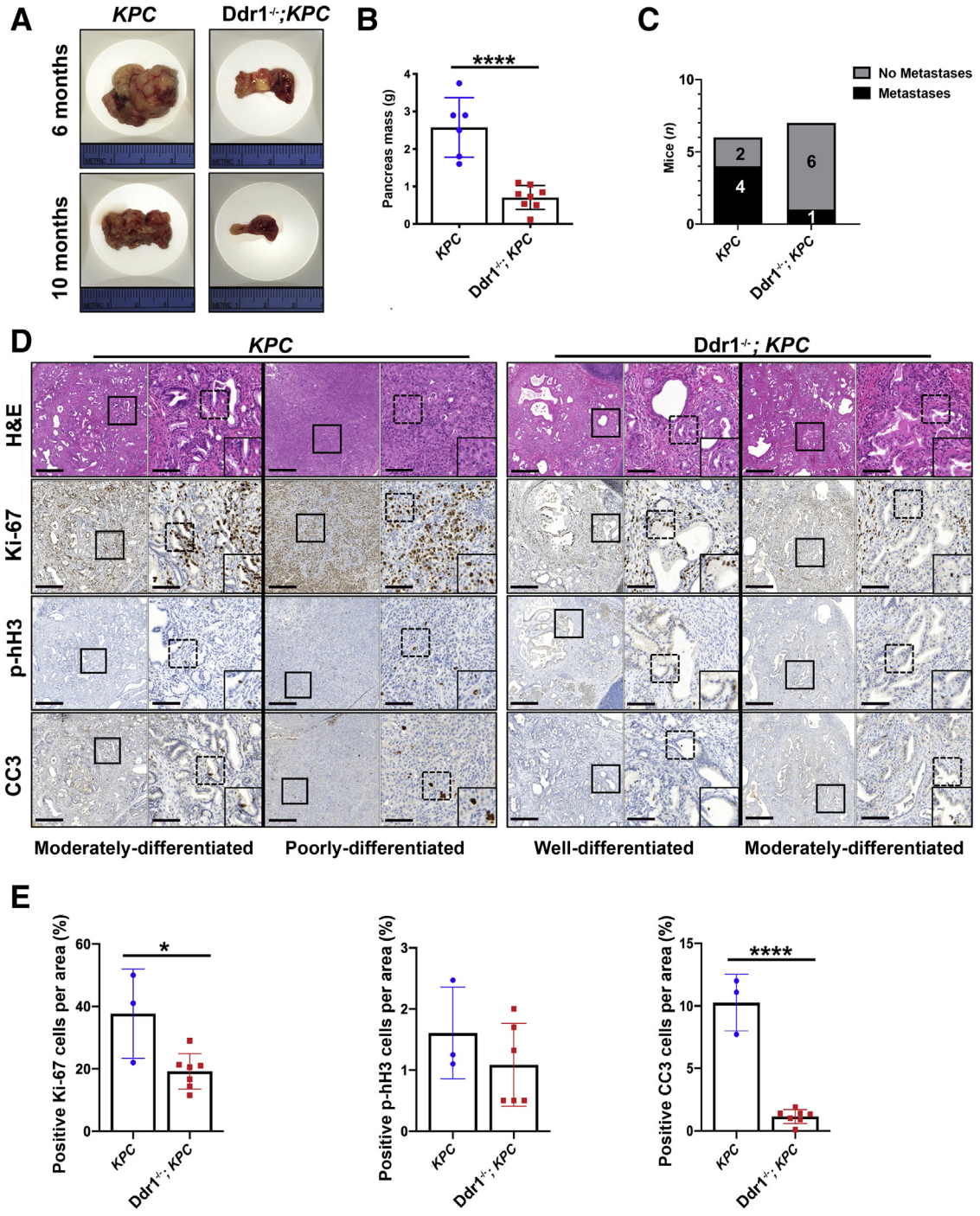

Figure 2 Discoidin domain receptor 1 (Ddr1) ablation reduces tumor growth and delays pancreatic ductal adenocarcinoma (PDA) progression. **A:** Gross anatomy of pancreata from *Kras*$^{G12D/+}$; *Trp53*$^{R172H/+}$; *Ptf1a*$^{Cre/+}$ (*KPC*) and Ddr1-null (*Ddr1*$^{-/-}$); *KPC* mice aged 6 and 10 months. **B:** Pancreatic mass of all *KPC* and *Ddr1*$^{-/-}$; *KPC* mice. **C:** Graphical representation of mice with macrometastasis to the liver. **D:** Histologic representation of moderately differentiated (far left) and poorly differentiated (middle, left) *KPC* pancreata along with well- (middle, right) and moderately- differentiated *Ddr1*$^{-/-}$; *KPC* pancreata. Low- and high-power images of specified areas for hematoxylin and eosin (H&E) (top), Ki-67, phosphohistone H3 (p-hH3), and cleaved caspase 3 (CC3) are shown with zoomed in images of each stain. **Solid boxed areas** are shown at higher magnification in the **right columns**; **dashed boxed areas** are shown at higher magnification in the **insets**. **E:** Quantification of respective staining for each group. Data are expressed as means ± SD. $n > 3$. *$P < 0.05$, ****$P < 0.0001$. Scale bars: 500 μm (**left columns**); 100 μm (**right columns**).

used as an indirect measure of neoplastic burden. At 2 months of age, when minimal transformation had occurred, *KC* and *Ddr1*$^{-/-}$; *KC* mice presented with similar PM/BW ratios of approximately 2%. By 1 year, this ratio reached approximately 3.5% in *KC* animals (Figure 4B). The PM/BW ratio in *Ddr1*$^{-/-}$; *KC* mice, in contrast, decreased to approximately 1.5% at the age of 1 year (Figure 4B). The decreased PM in *Ddr1*$^{-/-}$; *KC* mice did not reflect a delay

Table 2 *KPC* and *Ddr1*$^{-/-}$*; KPC* Tumor Grading

Genotype	Tumors, *n*		
	Well differentiated	Moderately differentiated	Poorly differentiated
KPC	0	3	3
Ddr1$^{-/-}$*; KPC*	3	3	1

Ddr1$^{-/-}$, discoidin domain receptor 1 null; *KPC*, *Kras*$^{G12D/+}$; *Trp53*$^{R172H/+}$; *Ptf1a*$^{Cre/+}$.

in the onset of transformation because both cohorts displayed a similar burden of ADM and PanIN lesions, as determined by H&E staining (Figure 4C). However, the two cohorts exhibited significant differences in other measures of pancreatic transformation. For instance, *Ddr1*$^{-/-}$*; KC* mice at 12 months of age had a greater reduction in normal acinar cell mass, as determined by IHC for the acinar cell marker amylase compared with controls (Figure 4, D and G). To determine the total area occupied by ADM and neoplasia, IHC for the duct cell marker cytokeratin-19 (CK19) was used but revealed no difference between the two cohorts (Figure 4, E and G). This finding suggests that the reduced PM in *Ddr1*$^{-/-}$*; KC* animals is primarily due to the loss of normal acinar tissue. *Ddr1*$^{-/-}$*; KC* mice also had fewer proliferating epithelial cells (p-hH3^{+}) as mice aged to 12 months compared with *KC* mice (Figure 4, F and H), a result similar to what we found in *Ddr1*$^{-/-}$*; KPC* tumors. Moreover, no differences in epithelial apoptosis (CC3^{+}) were observed between the cohorts at any age, again implicating an overall loss of proliferation as a primary cause of the difference in PM (Supplemental Figure S2C).

To examine fibrosis within the tissue, both *KC* and *Ddr1*$^{-/-}$*; KC* tissue were stained with Trichrome and Picrosirius Red, revealing no significant differences in fibrotic area at any time point (Supplemental Figure S2, D and E). This study also stained for collagen 1a (Col1a), the most prominent fibrillar collagen within the fibrotic stroma and a DDR1 ligand.[18] Again, no quantitative differences were observed in the total area of collagen deposition as measured by IHC for Col1a between the two cohorts as they aged to 12 months (Supplemental Figure S2F). Although no significant difference was found in fibrosis or Col1a staining, SHG microscopy revealed that levels of polymerized collagen fibers were significantly lower in *Ddr1*$^{-/-}$*; KC* mice at 12 months of age (Supplemental Figure S2G). This finding suggests that compared with the utility of DDR1 in tumor progression (Figure 3B), this ECM receptor may play a distinct role in collagen remodeling and polymerization in the stroma surrounding early neoplasia.

Experimental pancreatitis works synergistically with oncogenic Kras expression to accelerate tumorigenesis.[11,30] Consequently, the role of DDR1 in pancreatitis-associated tumorigenesis was examined. In this model, *KC* and *Ddr1*$^{-/-}$*; KC* mice were administered supramaximal doses

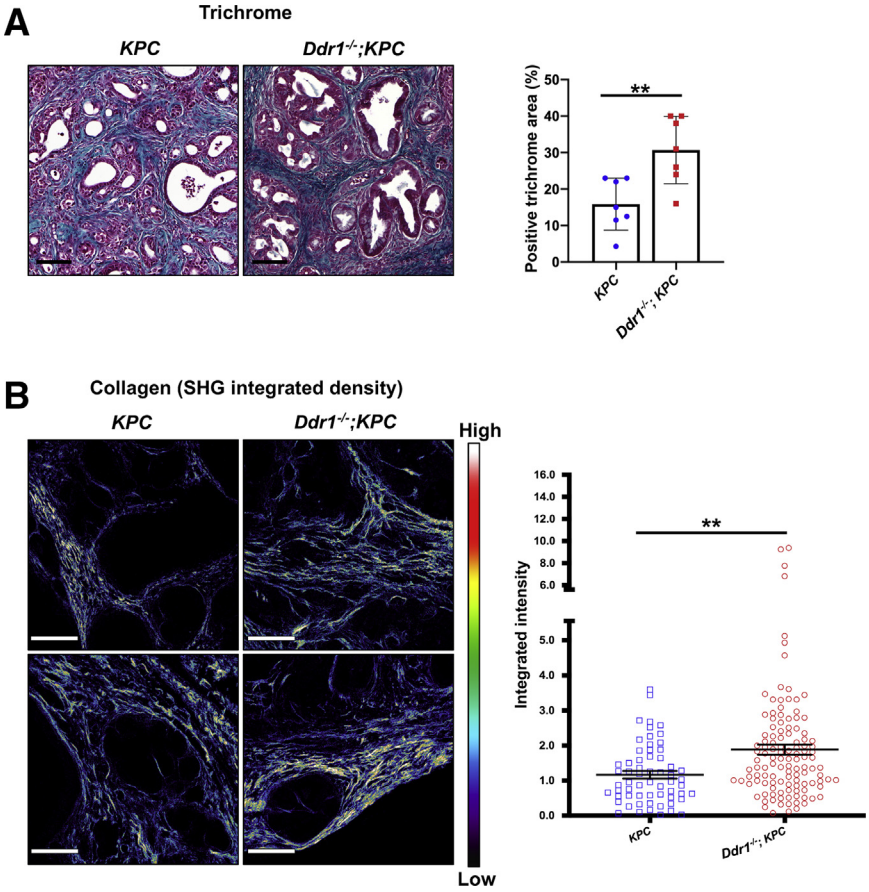

Figure 3 The absence of discoidin domain receptor 1 (Ddr1) alters the fibrotic response in pancreatic ductal adenocarcinoma PDA progression. **A:** Representative Trichrome staining (blue) of *Kras*$^{G12D/+}$*; Trp53*$^{R172H/+}$*; Ptf1a*$^{Cre/+}$ (*KPC*) (**left panel**) and Ddr1-null (*Ddr1*$^{-/-}$); *KPC* mice (**right panel**). Quantitative analysis of the percentage of positive Trichrome staining per tissue area shows *Ddr1*$^{-/-}$*; KPC* mice have significantly more fibrosis (graph on right). **B:** Representative images showing second harmonic generation (SHG) microscopy signatures from *KPC* mice (**left column**) and *Ddr1*$^{-/-}$*; KPC* (**right column**). Color scale indicates intensity of polymerized collagen fibers showing warm colors for high (white) and cold for low (black) SHG intensity levels. Quantitative analysis of polymerized collagen signatures (graph on right) obtained as SHG signal intensities divided by positive SHG signal areas (eg, integrated intensity). Values presented are relative (eg, normalized) to *KPC*. Data are expressed as means ± SD. $n > 3$ (5 for *KPC* and 6 for *Ddr1*$^{-/-}$*; KPC*) (**A**); $n = 9$ (3 selected areas from an H&E slide from each condition and 3 images/regions) (**B**). $^{**}P < 0.01$. Scale bars = 100 μm (**A** and **B**).

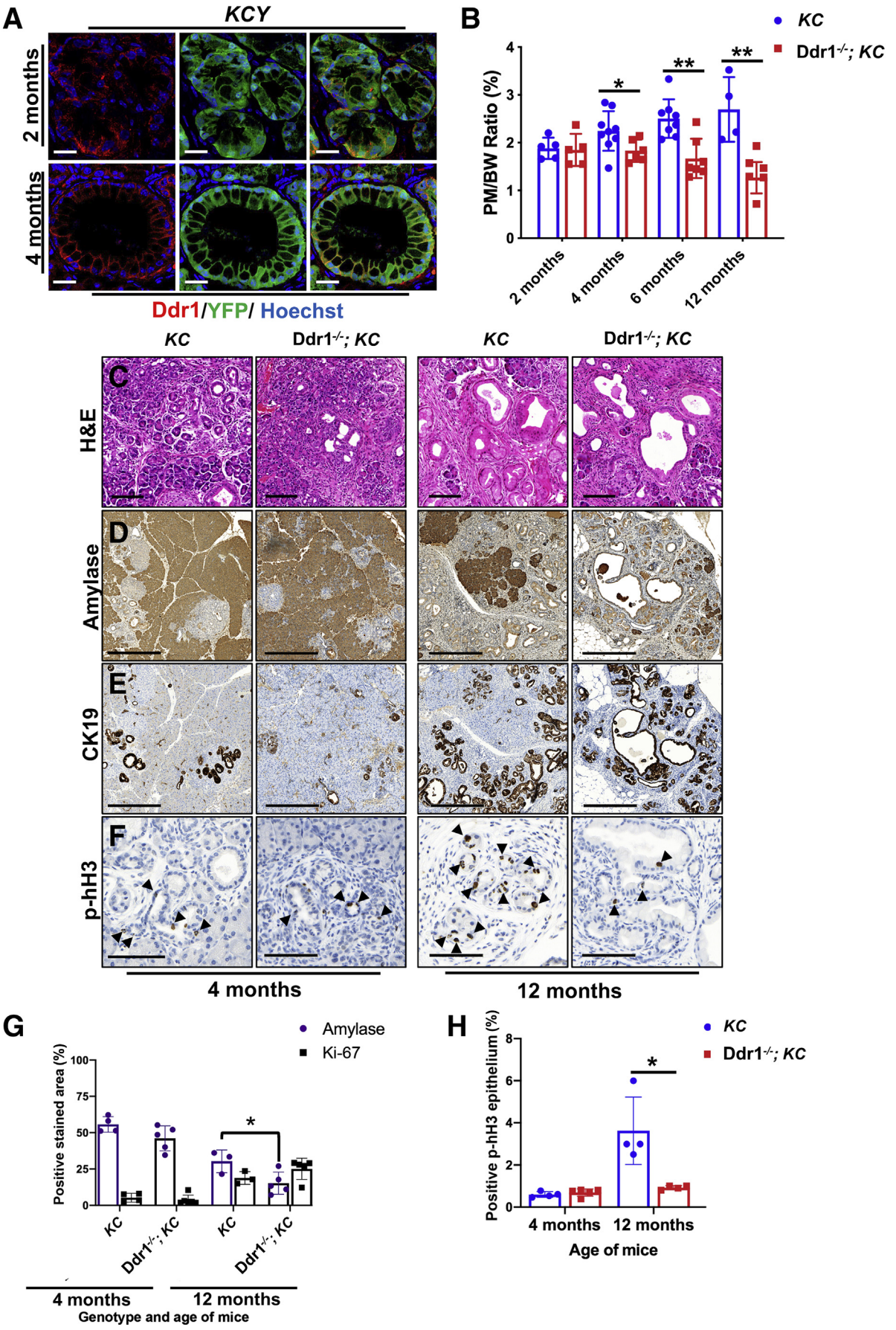
A
KCY
2 months
4 months
Ddr1/YFP/ Hoechst
B
KC
Ddr1-/-; KC
PM/BW Ratio (%)
2 months
4 months
6 months
12 months
KC
Ddr1-/-; KC
KC
Ddr1-/-; KC
C
H&E
D
Amylase
E
CK19
F
p-hH3
4 months
12 months
G
Amylase
Ki-67
Positive stained area (%)
KC
Ddr1-/-; KC
KC
Ddr1-/-; KC
4 months
12 months
Genotype and age of mice
H
KC
Ddr1-/-; KC
Positive p-hH3 epithelium (%)
4 months
12 months
Age of mice

of cerulein, a cholecystokinin ortholog, to induce acinar cell damage, resulting in pancreatitis.[30] Mice were treated once daily for 5 days with cerulein and sacrificed at 1, 4, and 6 weeks after the last injection (Figure 5A). One week after cerulein treatment, both cohorts had PM/BW ratios of approximately 3% to 4% (Figure 5B). However, as mice were allowed to recover, *KC* mice maintained a ratio of approximately 3%, whereas *Ddr1*$^{-/-}$*; KC* mice had a significant decrease in the PM/BW ratio, stabilizing at approximately 1% (Figure 5B). H&E staining showed a similar degree of tissue transformation at 1 week of recovery but revealed a failure to resolve tissue damage at 6 weeks after treatment in *Ddr1*$^{-/-}$*; KC* mice compared with *KC* mice (Supplemental Figure S3A). Loss of acinar tissue and its replacement by ADM/PanIN lesions in both *KC* and *Ddr1*$^{-/-}$*; KC* mice were measured by IHC for amylase and CK19, respectively (Figure 5, C, D, and G). Amylase-positive and CK19^{+} areas indicated that *KC* animals experienced widespread tissue damage and transformation but regained normal-appearing amylase^{+} acinar tissue by 6 weeks after cerulein treatment (Figure 5, C and G). In contrast, *Ddr1*$^{-/-}$*; KC* mice had little recovery of acinar tissue with a concomitant increase in CK19^{+} ductal cells (Figure 5, D and G).

These data reinforce that, in the absence of DDR1, the loss of normal tissue in a background of tumorigenesis and tissue damage contributes significantly to organ atrophy. Similar to observations in the *KPC* and spontaneous *KC* (Figure 4F) models, ablation of Ddr1 led to a less proliferative epithelium (p-hH3^{+}) (Figure 5, E and H) but no measurable difference in apoptotic cell death (CC3^{+}) (Supplemental Figure S3B). Tissue atrophy and the absence of acinar cells in *Ddr1*$^{-/-}$*; KC* pancreata was accompanied by a significant increase in Trichrome- and Picrosirius Red–positive stained area (Figure 5, F and I, and Supplemental Figure S3C). SHG signals revealed a more dynamic collagen polymerization and recovery rate in response to cerulein aggravation in the absence of DDR1, possibly highlighting a role for DDR1 in maintaining polymerized collagen stability (Supplemental Figure S3D). Taken together, the data from the spontaneous and pancreatitis-associated tumorigenesis models suggest that DDR1 is necessary for acinar cell homeostasis and regeneration, as well as for regulation of collagen deposition and polymerization.

DDR1 Is Necessary for Tissue Regeneration after Experimental Pancreatitis

Ablation of DDR1 in the *KPC* and *KC* mouse models consistently resulted in extensive tissue atrophy accompanied by stunted proliferation and an overall depletion of acinar cells. To further examine the effects of DDR1 ablation on pancreatic tissue homeostasis, we turned to a model of pancreatic injury in which supramaximal doses of cerulein were used to induce severe acute pancreatitis in *WT* and *Ddr1*$^{-/-}$ mice (Figure 6A). This treatment induces extensive ADM accompanied by a fibrotic response, similar to that found in CP. Unlike true CP, however, damage resolves in a period of several days after cerulein withdrawal.

After severe acute pancreatitis induction, Western blotting showed that Ddr1 expression was increased in *WT* mice during the tissue repair phase (Figure 6B). PM/BW ratios were used as an indirect measure of tissue injury and regeneration after cerulein treatment. On average, healthy pancreata from both *WT* and *Ddr1*$^{-/-}$ mice have PM/BW ratios of approximately 1.0% (Figure 6C). This ratio decreased to approximately 0.7% in *WT* mice 1 day after cerulein treatment but gradually recovered to approximately 1.0% after 2 weeks (Figure 6C). In comparison, *Ddr1*$^{-/-}$ mice had a more notable decrease in relative PM, decreasing below 0.5% with little recovery in tissue mass 2 weeks after cerulein cessation (Figure 6C). Gross anatomy reflected the smaller pancreata in *Ddr1*$^{-/-}$ mice (Supplemental Figure S4). H&E staining showed comparable initial damage between *WT* and *Ddr1*$^{-/-}$ mice, as indicated by the presence of ADM (Figure 6D). However, *Ddr1*$^{-/-}$ mice showed prolonged pancreatic damage at 7 days after treatment, which failed to return to a histologically normal phenotype until 2 weeks of recovery. Amylase^{+} staining confirmed that *Ddr1*$^{-/-}$ pancreata recovered their acinar cell population more slowly, with the most significant difference compared with *WT* pancreata at 7 days after cerulein treatment and no difference in CK19^{+} staining during recovery (Figure 6, E and F).

To examine the acute tissue atrophy and acinar cell loss in *DDR1*$^{-/-}$ mice, cell proliferation was next measured. In *WT* mice, an increase in Ki-67^{+} epithelia was evident 1 day after cerulein treatment and eventually subsided after 2 weeks when the tissue has recovered (Figure 7A). In contrast, Ddr1$^{-/-}$ mice experienced a delay in proliferation measured by fewer Ki-67^{+} epithelial cells at 1 and 3 days after cerulein treatment. Strikingly, the number of Ki-67^{+} epithelial cells significantly increases 7 days after cerulein treatment cessation, the timepoint that features the most significant decrease in pancreatic acinar mass but also when the tissue mass is stabilized in *WT* mice (Figure 7A). To test whether Ddr1 ablation affected acinar proliferation, co-immunofluorescence was performed for E-cadherin

Figure 4 Discoidin domain receptor 1 (Ddr1) is necessary for tissue homeostasis during tumorigenesis. **A:** Immunofluorescence detection of Ddr1 (red) at the membrane of acinar-ductal metaplasia in the the *Kras*$^{LSL\text{-}G12D/+}$*; Ptf1a*$^{Cre/+}$*; Rosa26R*$^{LSL\text{-}YFP/+}$ (*KCY*) mouse model at 2 and 4 months. The yellow fluorescent protein lineage tracer (green) and Hoechst (blue) for nuclear staining are shown. **B:** Pancreatic mass (PM)/body weight (BW) ratios of mice from 2, 4, 6, and 12 months of age. **C**–**F:** Representative immunohistochemical images for analysis in horizontal order of hematoxylin and eosin (H&E), amylase (brown), cytokeratin-19 (CK19) (brown), and phosphohistone H3 (p-hH3) (brown). **G:** Quantitative analysis of amylase and CK19 in control and Ddr1-null (Ddr1$^{-/-}$); *Kras*$^{G12D/+}$*; Ptf1a*$^{Cre/+}$ (*KC*) mice at 4 and 12 months of age. **H:** Quantitation of p-hH3 shows Ddr1$^{-/-}$*; KC* mice are less proliferative as they age and progress to neoplasia. Data are expressed as means ± SD. $n > 3$. *$P < 0.05$, **$P < 0.01$. Scale bars: 20 μm (**A**); 100 μm (**C**); 500 μm (**D** and **E**); 50 μm (**F**).

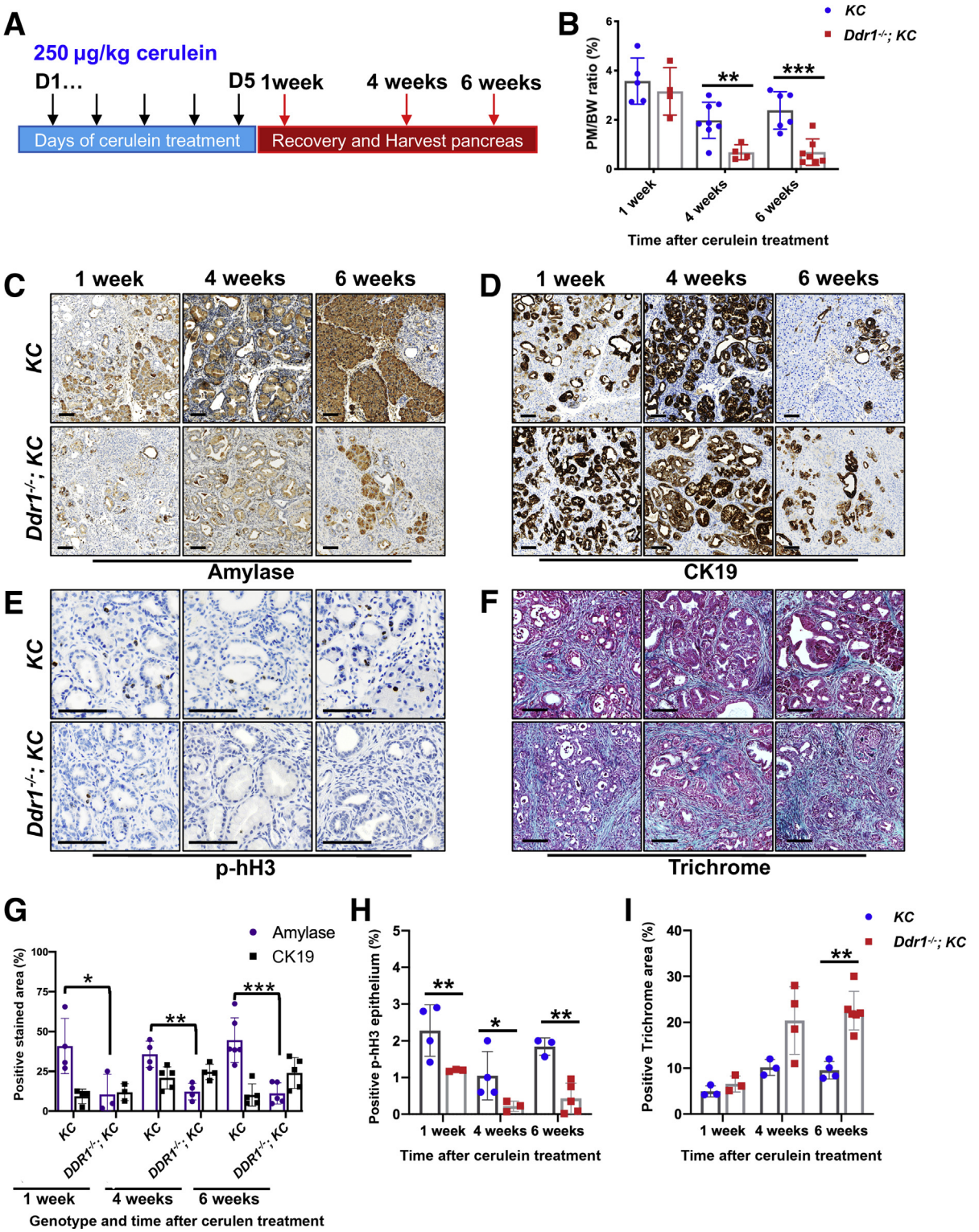

Figure 5 Discoidin domain receptor 1 (Ddr1) ablation disrupts tissue maintenance after pancreatitis-induced tumorigenesis. **A:** Schematic of cerulein treatment protocol and recovery period. **B:** Pancreatic mass (PM)/body weight (BW) ratios of mice at 1, 4, and 6 weeks after cerulein treatment **C**. **D:** Amylase and cytokeratin-19 (CK19) staining for control and Ddr1-null (*Ddr1*$^{-/-}$); *Kras*$^{G12D/+}$; *Ptf1a*$^{Cre/+}$ (*KC*) mice after cerulein treatment. Amylase (brown) decreases 1 month after cerulein treatment cessation but is recovered in controls after 6 weeks. Conversely, CK19 (brown) increases as amylase decreases in *Ddr1*$^{-/-}$; *KC* animals that maintain a loss in acinar population. **E:** Staining for phosphohistone H3 (p-hH3) (brown) shows significantly lower proliferation in *Ddr1*$^{-/-}$; *KC* animals 6 weeks after cerulein treatment. **F:** Trichrome (blue) increases during recovery phases for both cohorts but decreases in control compared with *Ddr1*$^{-/-}$; *KC* animals that maintain higher trichrome after 6 weeks. **G:** Graph of amylase and CK19 area quantitated from immunohistochemistry images. **H:** Quantitation of p-hH3. **I:** Quantitation of Trichrome. Data are expressed as means ± SD. $n > 3$. *$P < 0.05$, **$P < 0.01$, and ***$P < 0.001$. Scale bar = 100 µm (**C**–**F**).

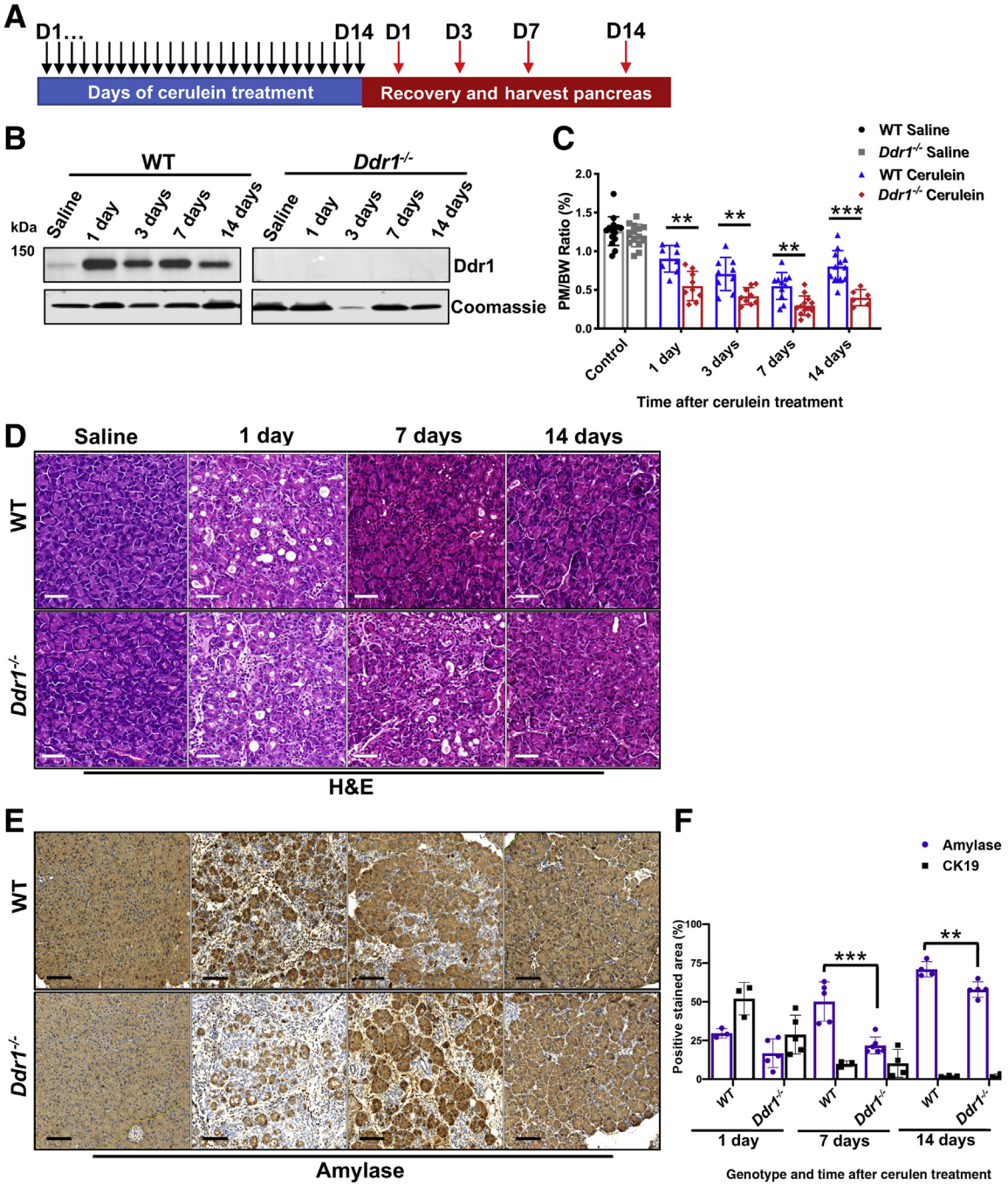

Figure 6 Discoidin domain receptor 1 (Ddr1) ablation impedes tissue recovery after cerulein-induced pancreatitis. **A:** Schematic of experimental pancreatitis protocol. **B:** Immunoblot for Ddr1 expression in wild-type (WT) and Ddr1-null (*Ddr1*$^{-/-}$) animals. WT animals have elevated Ddr1 during recovery. **C:** Pancreatic mass (PM)/body weight (BW) ratios of WT and *Ddr1*$^{-/-}$ mice at 1, 3, 7, and 14 days after 2 weeks of cerulein treatment. *Ddr1*$^{-/-}$ mice consistently have lower PM/BW ratios compared with control mice. **D:** Hematoxylin and eosin (H&E) images show healthy pancreata (top, saline controls) for WT and *Ddr1*$^{-/-}$. During recovery after cerulein treatment, controls and *Ddr1*$^{-/-}$ mice show evidence of tissue damage, with *Ddr1*$^{-/-}$ mice experiencing tissue damage 1 week after cerulein treatment compared with controls (right, center). **E:** Amylase (brown) staining for WT and *Ddr1*$^{-/-}$ reflects loss of tissue mass contributed toward a loss in amylase staining (acinar cells) during recovery, with more significant loss in staining in *Ddr1*$^{-/-}$ animals. **F:** Quantitation of amylase and cytokeratin-19 (CK19)—positive staining from immunohistochemistry images. Data are expressed as means ± SD. $n > 3$. $^{**}P < 0.01$, $^{***}P < 0.001$. Scale bar = 100 μm (**D** and **E**).

(epithelial marker), amylase (acinar cell marker), and p-hH3 (mitosis) (Figure 7B). p-hH3 staining was primarily located in the nuclei of E-cadherin^{+} and amylase^{+} cells in both *WT* and *Ddr1*$^{-/-}$ mice. As indicated by the extent of Ki-67 positivity, proliferative cells were numerous in *WT* pancreata during the early recovery time points but progressively decreased as homeostasis was restored. *Ddr1*$^{-/-}$ mice, however, had fewer proliferative epithelial cells at 1

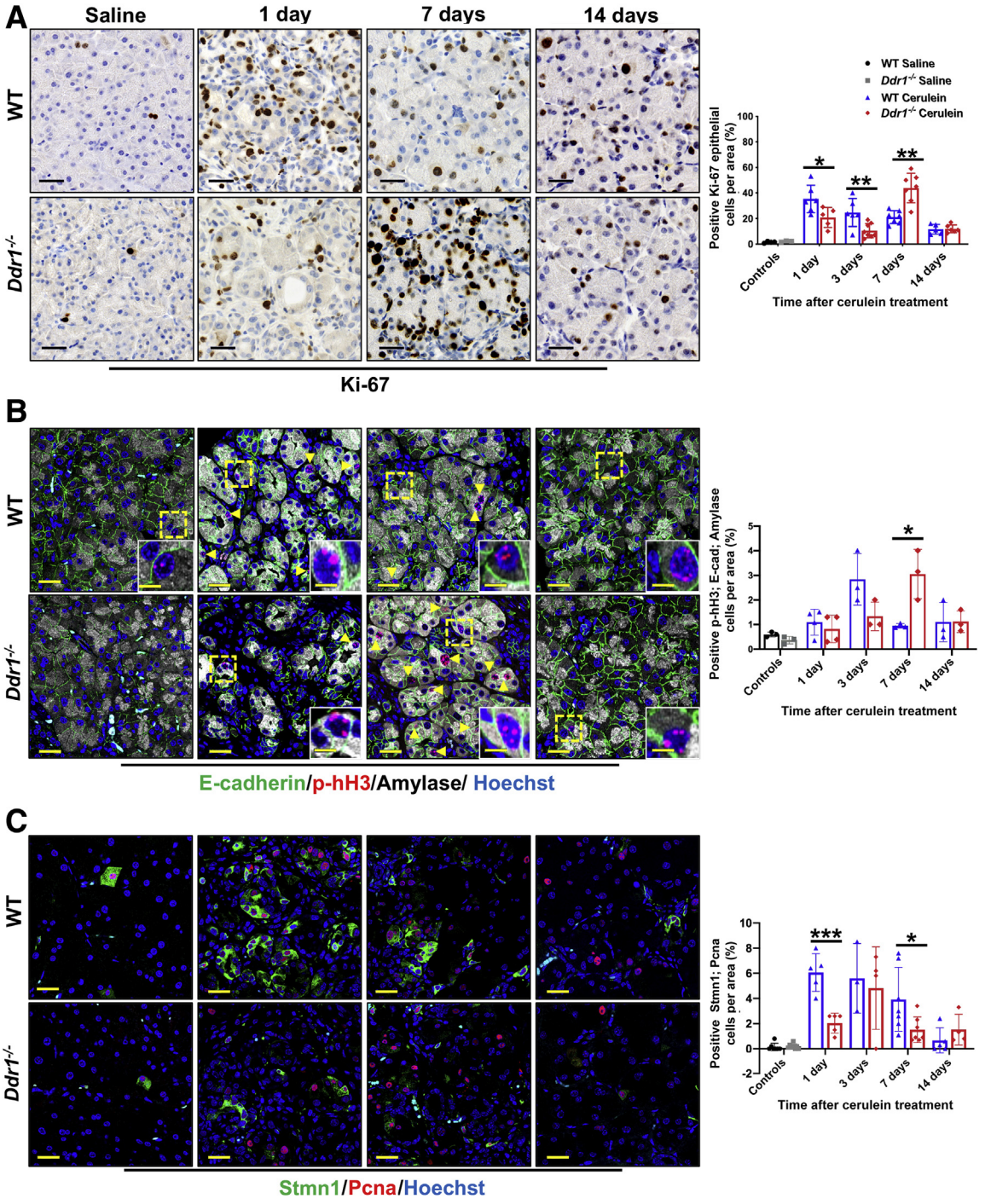

Figure 7 Proliferation is stunted during tissue recovery after cerulein treatment in discoidin domain receptor 1 (Ddr1) ablated mice. **A:** Ki-67 (brown) is detected in low amounts in saline controls (top, left). After cerulein treatment, controls have more Ki-67$^+$ epithelial up to 3 days of recovery (top, left center). Conversely, Ddr1-null (*Ddr1*$^{-/-}$) animals have lower Ki-67$^+$ epithelial cells at 1 and 3 (lower, left center) but a burst of Ki-67$^+$ cells 7 days after treatment (lower, right center). Both cohorts have similar Ki-67$^+$ cells 2 weeks after cerulein cessation (top and lower far left). Quantification of Ki-67 staining (right). **B:** Triple staining for E-cadherin (E-cad; green), amylase (white), phosphohistone H3 (p-hH3) (red), and nuclei (blue) to detect acinar cells undergoing mitosis. **Yellow triangles** indicate triple positive cells. **Boxed areas** are shown at higher magnification in the **insets**. Quantification of triple positive (E-cad$^+$, amylase$^+$, and p-hH3$^+$) cells (right). **C:** Co-staining for stathmin1 (Stmn1) (green), proliferating cell nuclear antigen (Pcna) (red), and nuclei (blue) to detect number of cells that contribute to the regeneration of the pancreas after injury. Double positive cells are detected in saline controls at low numbers. During recovery, the amount of Stmn1$^+$ and Pcna$^+$ cells increases in both WT and *Ddr1*$^{-/-}$ mice compared with saline controls, with significantly more cells in WT mice. Quantitation of dual positive (Stmn1$^+$ and Pcna$^+$) cell (right). Data are expressed as means ± SD. $n > 3$. *$P < 0.05$, **$P < 0.01$, and ***$P < 0.001$. Scale bars: 100 μm (**A** and **B**); 20 μm (**C**).

and 3 days, which markedly increased after 7 days of recovery (Figure 7B). As with the other models, we did not find a significant difference in the amount of apoptotic cell death between the cohorts, as measured by CC3 staining (Supplemental Figure S5).

After confirming a delay in cell proliferation following cerulein treatment in *Ddr1*$^{-/-}$ animals, it was hypothesized that this delay was attributable to a disruption in the regeneration potential of acinar cells during recovery. To test this hypothesis, tissues were stained for stathmin1 (Stmn1), which marks a subset of acinar cells that are uniquely capable of proliferation after pancreatic injury.[31] Co-staining for Stmn1 and proliferating cell nuclear antigen (Pcna) showed that WT and *Ddr1*$^{-/-}$ mice had similar numbers of Stmn1^{+} cells at baseline (saline control) (Figure 7C). However, after injury, WT mice had a large expansion of Stmn1^{+}; Pcna^{+} cells, an expansion that was delayed and then quickly subsided in *Ddr1*$^{-/-}$ mice (Figure 7C). These data suggest that the Stmn1^{+} subset of acinar cells is dependent on Ddr1 expression for its regenerative function, further reinforcing the critical role that Ddr1 plays in restoring pancreatic tissue homeostasis after injury.

The collagen-dense fibrotic response observed in pancreatic cancer is also a key feature in experimental and clinical pancreatitis.[4,27,32] To examine this, tissues from WT and *Ddr1*$^{-/-}$ mice were stained with Trichrome and Picrosirius Red. Both cohorts had an initial increase in Trichrome and Picrosirius Red staining 1 day after the experimental pancreatitis protocol (Figure 8A, Supplemental Figure S6A). As expected, WT tissues had a decrease in fibrosis as pancreata recovered from cerulein treatment, demonstrating tissue remodeling and a restoration of homeostatic equilibrium (Figure 8A, Supplemental Figure S6A). In contrast, *Ddr1*$^{-/-}$ mice failed to resolve the initial fibrosis 2 weeks after cerulein treatment, as indicated by the significantly higher amount of Trichrome, Picrosirius Red (Figure 8A, Supplemental Figure S6A), and Col1a staining (Figure 8B) in *Ddr1*$^{-/-}$ mice during the recovery phase. Finally, when assessing collagen polymerization dynamics via SHG microscopy, we confirmed that collagen fibrillogenesis was initially increased in *Ddr1*$^{-/-}$ animals 1 day after treatment. However, SHG signals decreased significantly at 3 and 7 days after cerulein treatment cessation in *Ddr1*$^{-/-}$ mice but failed to fully resolve compared with controls 2 weeks after treatment (Figure 8, C and D). The expression of several markers of fibrosis, including Ddr2, Col1a, and α-smooth muscle actin (activated fibroblasts) were also examined. Western blot analysis revealed increased amounts of these fibrotic markers in *Ddr1*$^{-/-}$ animals compared with WT cohorts. Furthermore, co-staining for the fibroblastic activation markers podoplanin and α-smooth muscle actin indicated a relative increase in the total number fibroblasts in *Ddr1*$^{-/-}$ animals during recovery after cerulein treatment, possibly explaining the failure of the tissue to fully resolve after injury (Supplemental Figure S6B).[33,34]

Discussion

The ECM is a three-dimensional network of protein polymers that are essential for the physical, biochemical, and mechanical support of organs.[35] In pancreatitis and PDA, the ECM undergoes a series of remodeling events that are orchestrated with the morphologic changes that occur in the epithelia throughout disease progression.[35] These changes are associated with an up-regulation of the expression of ECM proteins, infiltration of immune cells, and the activation of pancreatic stellate cells that secrete collagen to form the characteristic desmoplastic response observed in patients.[35,36] The desmoplastic reaction can influence the crosstalk between the microenvironment and tumor cells, affecting pancreatic disease progression.[3,35,36] However, selectively targeting stromal signaling pathways that promote pancreatic tumor progression without disturbing those that help constrain the tumor remains a challenge.[15,16]

Because of the late presentation of PDA, most patients are diagnosed with metastatic disease where the normal epithelium has been largely replaced by the collagen-rich desmoplasia, which subsequently increases organ stiffness and interstitial pressure, creating a barrier to the delivery of chemotherapy.[3,35,36] Several approaches have been used to target specific components of the ECM in pancreatic cancer. Although some show therapeutic promise, they have also revealed the complexity of the association between the stroma and cancer cells. Ablation of collagen-producing fibroblasts leads to a more aggressive tumor phenotype in both experimental and clinical studies.[14,15] As a result, other studies have attempted to modulate fibroblast activity and their production of ECM proteins, especially collagen, by targeting the inactivation of pancreatic stellate cells with vitamin D agonists.[17,37] Another approach in improving therapeutic delivery is to alleviate intratumoral pressure responsible for the collapse of the tumor vasculature by degrading hyaluronic acid, which is a prominent feature of the ECM of some patients with PDA.[38] The positive results from these preclinical studies led to clinical trials, culminating in a phase 3 trial in patients with high hyaluronic acid content, ultimately showing no benefit.[39] The lack of translational success so far emphasizes the need to better understand the complex dynamics of the tumor-stromal response in PDA progression.

The unique feature of the DDR family of type 1 receptor tyrosine kinases, namely the ability to signal in response to collagen ligands, suggests that these kinases may be a useful target for treating fibrotic diseases, including pancreatic cancer for which collagen is a dominant feature.[18] DDR1 is up-regulated in several cancers and fibrotic diseases, correlating with a worse prognosis. However, its role in cancer progression is complex and ill-defined.[18] Takai et al[21] ablated DDR1 in the MMTV-PyMT metastatic luminal-type

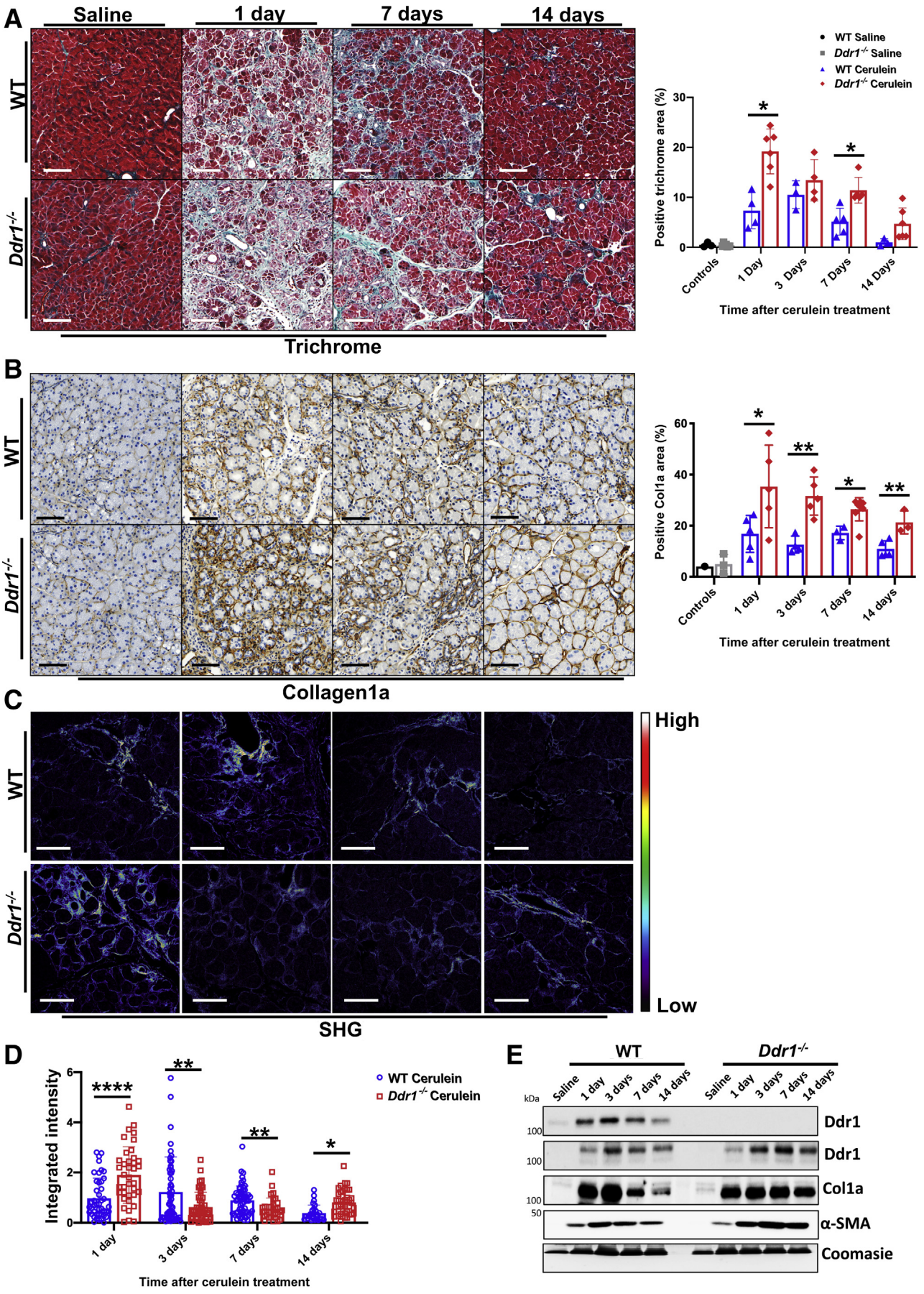
A
Saline
1 day
7 days
14 days
WT
Ddr1-/-
Trichrome
WT Saline
Ddr1-/- Saline
WT Cerulein
Ddr1-/- Cerulein
Positive trichrome area (%)
Controls
1 Day
3 Days
7 Days
14 Days
Time after cerulein treatment
B
Collagen1a
Positive Col1a area (%)
1 day
3 days
7 days
14 days
C
SHG
High
Low
D
Integrated intensity
WT Cerulein
Ddr1-/- Cerulein
E
WT
Ddr1-/-
kDa
Ddr1
Col1a
α-SMA
Coomasie

mammary tumor model and found that *DDR1*$^{-/-}$ tumors are more aggressive, fibrotic, and necrotic compared with controls. In contrast, Ambrogi et al[22] used *DDR1*$^{-/-}$ animals in the inducible *Kras*^{G12V} model of lung cancer, finding increased survival and reduced tumor size in *Ddr1*$^{-/-}$ mice. Similarly, the use of the DDR1 inhibitor 7rh in this model showed a significant reduction in tumor size when used in combination with Notch inhibitors.[22] Similarly, Aguilera et al[23] used 7rh to inhibit DDR1 in pancreatic cancer xenografts and the autochthonous *KPC* model and showed improved drug delivery in combination with gemcitabine, accompanied by a reduction in tumor burden and metastases. Together, these results suggest that the roles of DDR1 in cancer are context and organ dependent.

In our current studies, we used genetic ablation of Ddr1 (*Ddr1*$^{-/-}$) in several models that recapitulate the molecular and histologic events associated with pancreatitis, pancreatic neoplasia, and pancreatic cancer. Use of the metastatic *KPC* mouse model supported a role for DDR1 in pancreatic carcinoma progression to a poorly differentiated phenotype generally associated with an aggressive form of the cancer. Overshadowing possible effects on progression, tumor progression was accompanied by an unexpected and severe loss of PM in the absence of DDR1. In neoplasia, although DDR1 ablation had no obvious effects on transformation or fibrosis, it revealed severe tissue atrophy marked by a significant loss of normal acinar tissue. This effect was enhanced by accelerating transformation via induction of acute pancreatitis. The observed tissue atrophy was reminiscent of the phenotype seen when DDR1 was ablated in a mammary cancer model, in which the absence of DDR1 conferred a more fibrotic and necrotic tumor.[21] However, unlike that study, clear evidence of increased tissue necrosis (data not shown) was not observed. Finally, focusing solely on tissue damage, inducing severe acute pancreatitis in *DDR1*$^{-/-}$ animals recapitulated the severe tissue atrophy and acinar cell dropout that was similar to observations in the cancer and neoplastic models. In these cases, fibrosis and collagen deposition remained unresolved in the *DDR1*$^{-/-}$ mice for >1 week after cerulein treatment compared with controls, suggesting that DDR1 is necessary for ECM remodeling and is required for the restoration of normal homeostatic equilibrium after injury.

Exploring the tissue atrophy common to each model, no difference was found in the apoptotic index, measured by cleaved-caspase 3 IHC, or necrosis, measured by H&E (data not shown). Although several other mechanisms of cell death (eg, ferroptosis, necroptosis) were not measured, a modest increase in possible cellular senescence was seen, as measured by p21 IHC (data not shown). Most prominently, a decrease in epithelial proliferation in each DDR1 ablated model of pancreatic disease was consistently observed, which likely contributed to overall organ atrophy.

Although fibrosis constitutes a known feature of PDA onset and progression, stroma normalization (as opposed to desmoplastic elimination) is a highly sought clinical avenue.[17,40] However, fibrosis has also been reported as a predictor of improved survival in patients who underwent neoadjuvant therapy before surgery; in this case, increased levels of fibrosis observed at the time of surgery rendered improved outcomes in patients with PDA.[41] In addition, other studies suggest that the fibrotic stromal signatures could be indicative of improved or detrimental patient outcomes.[42,43] The varying outcomes from these studies suggest distinct protumor and antitumor types of fibrosis that are evident throughout the investigation of DDR1 activity in this study. The results attained from this study suggest a role for DDR1 in maintaining tissue homeostasis and demonstrate that the absence of DDR1 promotes dynamic ECM deposition and remodeling but prevents complete resolution after injury. Furthermore, these results encourage the notion that a tumoral homeostatic equilibrium is needed at each stage of tumorigenesis (eg, tumor onset and progression) and the absence of DDR1 prevents tissues from reaching these equilibria.

Collectively, these data indicate that DDR1 is an important signaling factor during pancreatic injury, tumor development, and tumor progression. These studies show that DDR1 is necessary for tissue homeostasis after an injury whether it be physical or oncogenic. Indeed, the ablation of DDR1 in pancreatic disease models in the current study had an impact on the surrounding desmoplasia, which usually exhibited a more persistent stromal response and altered rates of ECM remodeling. Altogether, the overexpression of DDR1 and the extensive collagen production in pancreatic diseases suggest that DDR1 is a putative therapeutic target. However, these results also suggest that long-term systemic inhibition of DDR1 could induce organ atrophy in an environment of chronic cell stress, a factor that should be taken into account when targeting DDR1.

Figure 8 Discoidin domain receptor 1 (Ddr1)—null (*Ddr1*$^{-/-}$) mice develop extensive fibrosis after pancreatic injury. **A:** Trichrome (blue/green) staining in both control and *Ddr1*$^{-/-}$ animals is elevated, but significantly more fibrosis occurs in *Ddr1*$^{-/-}$ mice (left). Quantitation of Trichrome staining (right). **B:** Collagen 1a (Col1a) staining reflects the increased Trichrome staining, with *Ddr1*$^{-/-}$ mice having more Col1a present during recovery (left). Quantitation of Col1a staining (right). **C:** Representative images of second harmonic generation (SHG) during recovery after pancreatic injury reveal increased signals indicative of polymerized collagen deposition in *Ddr1*$^{-/-}$ mice. Warm colors represent areas of denser collagen fibrils. **D:** Quantitation of SHG shows that the increased fibrillogenesis remained unresolved in *Ddr1*$^{-/-}$ mice 2 weeks after cerulein treatment. **E:** Western blot analysis of whole tissue lysates for common markers of fibrosis. Data are expressed as means ± SD. $n > 3$ [**A** and **B**; 3 for wild-type (WT) and 3 for *Ddr1*$^{-/-}$ mice per timepoint]; $n = 9$ (**D**; 3 selected areas from each condition and 3 images/regions). *$P < 0.05$, **$P < 0.01$, and ****$P < 0.0001$. Scale bars = 100 μm (**A**–**C**). SMA, α-smooth muscle actin.

Supplemental Data

Supplemental material for this article can be found at *http://doi.org/10.1016/j.ajpath.2020.03.020*.

References

1. Siegel RL, Miller KD, Jemal A: Cancer statistics, 2020. CA Cancer J Clin 2020, 70:7–30
2. Collisson EA, Bailey P, Chang DK, Biankin AV: Molecular subtypes of pancreatic cancer. Nat Rev Gastroenterol Hepatol 2019, 16: 207–220
3. Neoptolemos JP, Kleeff J, Michl P, Costello E, Greenhalf W, Palmer DH: Therapeutic developments in pancreatic cancer: current and future perspectives. Nat Rev Gastroenterol Hepatol 2018, 15: 333–348
4. Witt H, Apte MV, Keim V, Wilson JS: Chronic pancreatitis: challenges and advances in pathogenesis, genetics, diagnosis, and therapy. Gastroenterology 2007, 132:1557–1573
5. Strobel O, Dor Y, Alsina J, Stirman A, Lauwers G, Trainor A, Castillo CF, Warshaw AL, Thayer SP: In vivo lineage tracing defines the role of acinar-to-ductal transdifferentiation in inflammatory ductal metaplasia. Gastroenterology 2007, 133:1999–2009
6. Desai BM, Oliver-Krasinski J, De Leon DD, Farzad C, Hong N, Leach SD, Stoffers DA: Preexisting pancreatic acinar cells contribute to acinar cell, but not islet beta cell, regeneration. J Clin Invest 2007, 117:971–977
7. Hidalgo-Sastre A, Brodylo RL, Lubeseder-Martellato C, Sipos B, Steiger K, Lee M, von Figura G, Grunwald B, Zhong S, Trajkovic-Arsic M, Neff F, Schmid RM, Siveke JT: Hes1 controls exocrine cell plasticity and restricts development of pancreatic ductal adenocarcinoma in a mouse model. Am J Pathol 2016, 186:2934–2944
8. Kopp JL, von Figura G, Mayes E, Liu FF, Dubois CL, Morris JPt, Pan FC, Akiyama H, Wright CV, Jensen K, Hebrok M, Sander M: Identification of Sox9-dependent acinar-to-ductal reprogramming as the principal mechanism for initiation of pancreatic ductal adenocarcinoma. Cancer Cell 2012, 22:737–750
9. Søreide K, Primavesi F, Labori KJ, Watson MM, Stättner S: Molecular biology in pancreatic ductal adenocarcinoma: implications for future diagnostics and therapy. Eur Surg 2019, 51:126–134
10. Iacobuzio-Donahue CA: Genetic evolution of pancreatic cancer: lessons learnt from the pancreatic cancer genome sequencing project. Gut 2012, 61:1085–1094
11. Guerra C, Schuhmacher AJ, Canamero M, Grippo PJ, Verdaguer L, Perez-Gallego L, Dubus P, Sandgren EP, Barbacid M: Chronic pancreatitis is essential for induction of pancreatic ductal adenocarcinoma by K-Ras oncogenes in adult mice. Cancer Cell 2007, 11: 291–302
12. Halbrook CJ, Pasca di Magliano M, Lyssiotis CA: Tumor cross-talk networks promote growth and support immune evasion in pancreatic cancer. Am J Physiol Gastrointest Liver Physiol 2018, 315:G27–G35
13. Provenzano PP, Cuevas C, Chang AE, Goel VK, Von Hoff DD, Hingorani SR: Enzymatic targeting of the stroma ablates physical barriers to treatment of pancreatic ductal adenocarcinoma. Cancer Cell 2012, 21:418–429
14. Olive KP, Jacobetz MA, Davidson CJ, Gopinathan A, McIntyre D, Honess D, et al: Inhibition of Hedgehog signaling enhances delivery of chemotherapy in a mouse model of pancreatic cancer. Science 2009, 324:1457–1461
15. Ozdemir BC, Pentcheva-Hoang T, Carstens JL, Zheng X, Wu CC, Simpson TR, Laklai H, Sugimoto H, Kahlert C, Novitskiy SV, De Jesus-Acosta A, Sharma P, Heidari P, Mahmood U, Chin L, Moses HL, Weaver VM, Maitra A, Allison JP, LeBleu VS, Kalluri R: Depletion of carcinoma-associated fibroblasts and fibrosis induces immunosuppression and accelerates pancreas cancer with reduced survival. Cancer Cell 2014, 25:719–734
16. Rhim AD, Oberstein PE, Thomas DH, Mirek ET, Palermo CF, Sastra SA, Dekleva EN, Saunders T, Becerra CP, Tattersall IW, Westphalen CB, Kitajewski J, Fernandez-Barrena MG, Fernandez-Zapico ME, Iacobuzio-Donahue C, Olive KP, Stanger BZ: Stromal elements act to restrain, rather than support, pancreatic ductal adenocarcinoma. Cancer Cell 2014, 25:735–747
17. Sherman MH, Yu RT, Engle DD, Ding N, Atkins AR, Tiriac H, Collisson EA, Connor F, Van Dyke T, Kozlov S, Martin P, Tseng TW, Dawson DW, Donahue TR, Masamune A, Shimosegawa T, Apte MV, Wilson JS, Ng B, Lau SL, Gunton JE, Wahl GM, Hunter T, Drebin JA, O'Dwyer PJ, Liddle C, Tuveson DA, Downes M, Evans RM: Vitamin D receptor-mediated stromal reprogramming suppresses pancreatitis and enhances pancreatic cancer therapy. Cell 2014, 159:80–93
18. Leitinger B: Discoidin domain receptor functions in physiological and pathological conditions. Int Rev Cell Mol Biol 2014, 310: 39–87
19. Avivi-Green C, Singal M, Vogel WF: Discoidin domain receptor 1-deficient mice are resistant to bleomycin-induced lung fibrosis. Am J Respir Crit Care Med 2006, 174:420–427
20. Guerrot D, Kerroch M, Placier S, Vandermeersch S, Trivin C, Mael-Ainin M, Chatziantoniou C, Dussaule JC: Discoidin domain receptor 1 is a major mediator of inflammation and fibrosis in obstructive nephropathy. Am J Pathol 2011, 179:83–91
21. Takai K, Drain AP, Lawson DA, Littlepage LE, Karpuj M, Kessenbrock K, Le A, Inoue K, Weaver VM, Werb Z: Discoidin domain receptor 1 (Ddr1) ablation promotes tissue fibrosis and hypoxia to induce aggressive basal-like breast cancers. Genes Dev 2018, 32:244–257
22. Ambrogio C, Gomez-Lopez G, Falcone M, Vidal A, Nadal E, Crosetto N, Blasco RB, Fernandez-Marcos PJ, Sanchez-Cespedes M, Ren X, Wang Z, Ding K, Hidalgo M, Serrano M, Villanueva A, Santamaria D, Barbacid M: Combined inhibition of Ddr1 and Notch signaling is a therapeutic strategy for KRAS-driven lung adenocarcinoma. Nat Med 2016, 22:270–277
23. Aguilera KY, Huang H, Du W, Hagopian MM, Wang Z, Hinz S, Hwang TH, Wang H, Fleming JB, Castrillon DH, Ren X, Ding K, Brekken RA: Inhibition of discoidin domain receptor 1 reduces collagen-mediated tumorigenicity in pancreatic ductal adenocarcinoma. Mol Cancer Ther 2017, 16:2473–2485
24. Hou G, Vogel W, Bendeck MP: The discoidin domain receptor tyrosine kinase DDR1 in arterial wound repair. J Clin Invest 2001, 107:727–735
25. Hingorani SR, Petricoin EF, Maitra A, Rajapakse V, King C, Jacobetz MA, Ross S, Conrads TP, Veenstra TD, Hitt BA, Kawaguchi Y, Johann D, Liotta LA, Crawford HC, Putt ME, Jacks T, Wright CV, Hruban RH, Lowy AM, Tuveson DA: Preinvasive and invasive ductal pancreatic cancer and its early detection in the mouse. Cancer Cell 2003, 4:437–450
26. Hingorani SR, Wang L, Multani AS, Combs C, Deramaudt TB, Hruban RH, Rustgi AK, Chang S, Tuveson DA: Trp53R172H and KrasG12D cooperate to promote chromosomal instability and widely metastatic pancreatic ductal adenocarcinoma in mice. Cancer Cell 2005, 7:469–483
27. Halbrook CJ, Wen HJ, Ruggeri JM, Takeuchi KK, Zhang Y, di Magliano MP, Crawford HC: Mitogen-activated protein kinase kinase activity maintains acinar-to-ductal metaplasia and is required for organ regeneration in pancreatitis. Cell Mol Gastroenterol Hepatol 2017, 3:99–118
28. Flamant M, Placier S, Rodenas A, Curat CA, Vogel WF, Chatziantoniou C, Dussaule JC: Discoidin domain receptor 1 null mice are protected against hypertension-induced renal disease. J Am Soc Nephrol 2006, 17:3374–3381
29. Thomas D, Radhakrishnan P: Tumor-stromal crosstalk in pancreatic cancer and tissue fibrosis. Mol Cancer 2019, 18:14

30. Ardito CM, Gruner BM, Takeuchi KK, Lubeseder-Martellato C, Teichmann N, Mazur PK, Delgiorno KE, Carpenter ES, Halbrook CJ, Hall JC, Pal D, Briel T, Herner A, Trajkovic-Arsic M, Sipos B, Liou GY, Storz P, Murray NR, Threadgill DW, Sibilia M, Washington MK, Wilson CL, Schmid RM, Raines EW, Crawford HC, Siveke JT: EGF receptor is required for KRAS-induced pancreatic tumorigenesis. Cancer Cell 2012, 22:304−317
31. Wollny D, Zhao S, Everlien I, Lun X, Brunken J, Brune D, Ziebell F, Tabansky I, Weichert W, Marciniak-Czochra A, Martin-Villalba A: Single-cell analysis uncovers clonal scinar cell heterogeneity in the adult pancreas. Dev Cell 2016, 39:289−301
32. Wen HJ, Gao S, Wang Y, Ray M, Magnuson MA, Wright CVE, Di Magliano MP, Frankel TL, Crawford HC: Myeloid cell-derived HB-EGF drives tissue recovery after pancreatitis. Cell Mol Gastroenterol Hepatol 2019, 8:173−192
33. Astarita JL, Acton SE, Turley SJ: Podoplanin: emerging functions in development, the immune system, and cancer. Front Immunol 2012, 3:283
34. Elyada E, Bolisetty M, Laise P, Flynn WF, Courtois ET, Burkhart RA, Teinor JA, Belleau P, Biffi G, Lucito MS, Sivajothi S, Armstrong TD, Engle DD, Yu KH, Hao Y, Wolfgang CL, Park Y, Preall J, Jaffee EM, Califano A, Robson P, Tuveson DA: Cross-species single-cell analysis of pancreatic ductal adenocarcinoma reveals antigen-presenting cancer-associated fibroblasts. Cancer Discov 2019, 9:1102−1123
35. Weniger M, Honselmann KC, Liss AS: The extracellular matrix and pancreatic cancer: a complex relationship. Cancers (Basel) 2018, 10:316
36. Ahn DH, Ramanathan RK, Bekaii-Saab T: Emerging therapies and future directions in targeting the tumor stroma and immune system in the treatment of pancreatic adenocarcinoma. Cancers (Basel) 2018, 10:193
37. Chronopoulos A, Robinson B, Sarper M, Cortes E, Auernheimer V, Lachowski D, Attwood S, Garcia R, Ghassemi S, Fabry B, Del Rio Hernandez A: ATRA mechanically reprograms pancreatic stellate cells to suppress matrix remodelling and inhibit cancer cell invasion. Nat Commun 2016, 7:12630
38. Hingorani SR, Harris WP, Beck JT, Berdov BA, Wagner SA, Pshevlotsky EM, Tjulandin SA, Gladkov OA, Holcombe RF, Korn R, Raghunand N, Dychter S, Jiang P, Shepard HM, Devoe CE: Phase Ib study of PEGylated recombinant human hyaluronidase and gemcitabine in patients with advanced pancreatic cancer. Clin Cancer Res 2016, 22:2848−2854
39. Hakim N, Patel R, Devoe C, Saif MW: Why HALO 301 failed and implications for treatment of pancreatic cancer. Pancreas (Fairfax) 2019, 3:e1−e4
40. Jiang H, Hegde S, Knolhoff BL, Zhu Y, Herndon JM, Meyer MA, Nywening TM, Hawkins WG, Shapiro IM, Weaver DT, Pachter JA, Wang-Gillam A, DeNardo DG: Targeting focal adhesion kinase renders pancreatic cancers responsive to checkpoint immunotherapy. Nat Med 2016, 22:851−860
41. Sasson AR, Wetherington RW, Hoffman JP, Ross EA, Cooper H, Meropol NJ, Freedman G, Pingpank JF, Eisenberg BL: Neoadjuvant chemoradiotherapy for adenocarcinoma of the pancreas: analysis of histopathology and outcome. Int J Gastrointest Cancer 2003, 34: 121−128
42. Erkan M, Michalski CW, Rieder S, Reiser-Erkan C, Abiatari I, Kolb A, Giese NA, Esposito I, Friess H, Kleeff J: The activated stroma index is a novel and independent prognostic marker in pancreatic ductal adenocarcinoma. Clin Gastroenterol Hepatol 2008, 6:1155−1161
43. Franco-Barraza J, Francescone R, Luong T, Shah N, Madhani R, Cukierman G, Dulaimi E, Devarajan K, Egleston BL, Nicolas E, Katherine Alpaugh R, Malik R, Uzzo RG, Hoffman JP, Golemis EA, Cukierman E: Matrix-regulated integrin alphavbeta5 maintains alpha5beta1-dependent desmoplastic traits prognostic of neoplastic recurrence. Elife 2017, 6:e20600